https://doi.org/10.1007/s41230-021-0141-8

Internal shrinkage crack in a 10 t water-cooled steel ingot with a large height-to-diameter ratio

***Jing-an Yang[1], Hou-fa Shen[2]**

1. School of Transportation Science and Engineering, Beihang University, Beijing 100191, China

2. School of Materials Science and Engineering, Tsinghua University, Beijing 100084, China

Abstract: Steel ingot with a large height-to-diameter ratio is utilized to produce multiple products by one stock in practice. Water cooling is a usual way to enhance production efficiency. However, the combination of the two factors will generate internal defects, such as shrinkage porosity and hot crack. The characteristic of internal shrinkage crack in a 10 t water-cooled steel ingot with a large height-to-diameter ratio was examined by an ultrasonic test. A slice was sectioned from the ingot middle part where billets containing star-like crack were further extracted. The billets were examined by X-ray high energy industrial CT, and the compactness was reconstructed in three dimensions. Microstructure near the crack was observed using scanning electron microscopy, and the solidification process and grain size were studied by high temperature confocal microscopy. Moreover, thermo-mechanical simulation and post-processing were carried out to analyze the formation of shrinkage porosity and hot crack. A new criterion considering mushy zone mechanical behavior in brittle temperature as well as grain size distribution was proposed to evaluate hot cracking potential in the ingot. The results show that a deep shrinkage porosity band easily forms in the center line of such an ingot with a large height-to-diameter ratio, and water-cooling further generates excessive tensile stress tearing the liquid films around the porosities. Then, hot cracks begin to propagate along grain boundaries. The grain size in the upper and center of the ingot is large, which leads to an inverted cone shape defects zone in the ingot center.

Key words: steel ingot; porosity; hot crack; industrial CT; thermo-mechanical simulation

CLC numbers: TG142.1/TP391.9 **Document code:** A **Article ID:** 1672-6421(2021)02-110-08

1 Introduction

Water-cooled mold casting technology has potential advantages to increase the cooling strength, shorten the solidification time, and refine the macrostructure of the ingot, so as to improve the quality and production rate. Liu et al. [1] investigated the 5 t steel ingots cast in sand molds with and without water cooling, and found that the water-cooled ingot has a less intensive macrosegregation. Meng et al. [2] studied a 3.3 t water-cooled steel ingot, and concluded that when the cooling rate is below 1,000 $W \cdot m^{-2} \cdot k^{-1}$, increasing the cooling rate can significantly reduce the melt flow velocity, the mushy zone width and solidification time, and alleviate macrosegregation of the ingot. Zhao et al. [3] cast M2 steel ingots by the water-cooled copper mold and the sand mold, and pointed out that water-cooling could obtain more uniform and finer grains. Wen et al. [4] prepared a 45 t steel ingot with a water-cooled chassis, and suggested that strengthening the bottom cooling can balance the solidification front of molten steel, normalize the air gap distribution, and improve the ingot quality.

Raising the height-to-diameter ratio of the ingot is another effective way to improve utilization rate of the ingot. Tyurin et al.[5] created newly designed molds to achieve horizontal crystallization of the steel, and cast long ingots with a height-to-diameter ratio as large as 9, indicating that under a properly controlled cooling boundary condition, high quality large height-to-diameter ratio ingots can be made. Chen et al.[6] stated that it is difficult to achieve a long-range liquid feeding for the casting with a large height-to-diameter ratio, and proposed a solid feeding mechanism. Yu et al.[7] analyzed the heat transfer resistances at different solidification stages of an 18 t steel ingot with a large height-to-diameter ratio, and stressed that heat transfer of the solidified shell is the main restrictive step in the whole solidification process.

It is a challenge to apply water-cooled mold casting technology to a steel ingot with a large height-to-

***Jing-an Yang**

Male, born in 1987, Ph. D. Research interests: modeling and simulation of the solidification process related to casting.

E-mail: jinganyang8992@buaa.edu.cn;

Received: 2020-10-14; Accepted: 2021-02-22

diameter ratio due to its difficulties in process parameter control for mass feeding. Common ingot defects, such as shrinkage porosity and hot crack, are main concerns. To predict these defects, scholars worldwide have done a lot of research works and put forward many models and criteria [8-13]. Niyama et al. [14] proposed a criterion for shrinkage porosity through casting steel cylinders of different diameters. Hardin et al. [15, 16] studied the influence of pore distribution on mechanical properties of cast steel by experiment and simulation, and found that the ductility of porous cast steel deceases significantly with the increase of porosity. Won et al. [17] indicated that in the brittle temperature range (BTR), the existence of liquid film between dendrites increases the risk of hot cracking in the mushy zone. Stangeland et al. [18] established a two-phase model of a volume average method to simulate hot cracking tendency of castings, and pointed out that insufficient feeding and excessive deformation in the high solid fraction region are the main causes of hot cracking. A 6 t normal ingot was sliced to ascertain the internal quality [19]. Numerical simulation revealed that hot crack develops only when stress and strain exceed a threshold value within the brittle temperature range. Recently, a 234 t ingot was dissected and a shrinkage crack potential criterion considering shrinkage porosity as well as mushy zone mechanical property was proposed [20]. However, grain size, which is influenced by the cooling intensity, was rarely considered in the hot cracking potential (HCP) criterion.

In this study, a 10 t water-cooled steel ingot with a large height-to-diameter ratio was studied by ultrasonic inspection, CT imaging, scanning electron microscopy (SEM), and high temperature confocal microscopy. Then, thermo-mechanical simulation and post-processing were carried out to analyze the internal shrinkage crack with a new hot cracking potential criterion, considering grain size distribution and mushy zone mechanical behavior within the brittle temperature range.

2 Experiment

Figure 1 shows the schematic of the water-cooled steel ingot mold system, including water pump, water tank, motor and control system, in which a water channel was set between the ingot inner mold and outer mold.

The 10 t water-cooled ingot was made of P91 heat resistant steel with the composition shown in Table 1. The ingot shape was nearly a cone with the height of 3,180 mm, the upper diameter 820 mm, and the lower diameter 550 mm, i.e., the height-to-diameter ratio was 4.64, and the taper was 8.5%. Bottom pouring was used in the casting process with the pouring temperature of 1,550 °C and the filling speed in ingot body and riser of 16 $kg \cdot s^{-1}$ and 8 $kg \cdot s^{-1}$, respectively. The exothermic compound and anti-piping compound were added with the heating capacity of 8,000 $kJ \cdot kg^{-1}$. The cooling water flow rate was 380 $m^3 \cdot h^{-1}$, and decreased to 230 $m^3 \cdot h^{-1}$ after one hour. The demolding time was 3.2 h.

Table 1: Composition of P91 grade steel (wt.%)

C	Si	Mn	V	Cr	Mo	S	P	Nb	Fe
0.099	0.2	0.3	0.18	8	0.9	0.000955	0.001	0.06	Bal.

2.1 Ultrasonic inspection

Ultrasonic inspection was carried out on the 10 t water-cooled steel ingot. Defects were found 480 mm below the riser and 180 mm above the ingot bottom with the average depth to surface of 150 mm. The defect area shape was an inverted cone with the upper part wide and lower part narrow, as in the red dashed area shown in Fig. 2.

2.2 Sampling

A short stock with diameter of 650 mm and thickness of 50 mm was cut from the cross section of the ingot by sawing machine, which was 2,260 mm above the ingot bottom as indicated by the purple rim shown in Fig. 2. A star shaped defect with diameter of about 80 mm in the stock center was found as seen in the marked red circle in Fig. 3.

Then the stock was further meshed and cubic billets with the side size of 20 mm were prepared for X-ray high energy industrial CT as shown in Fig. 4.

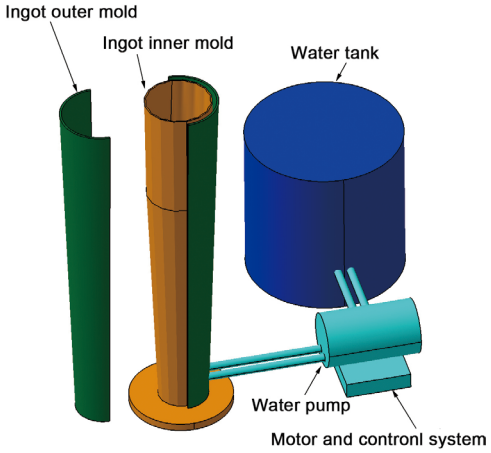

Fig. 1: Schematic of water-cooled steel ingot mold system

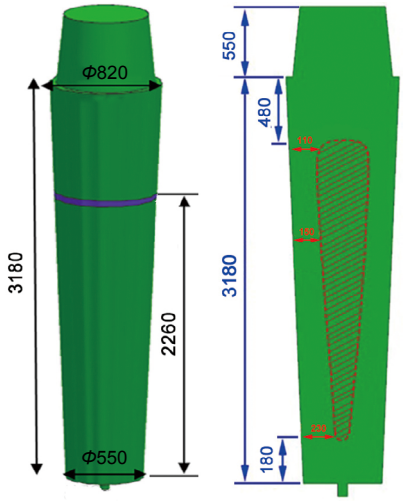

Fig. 2: Defects distribution in ingot with ultrasonic test (unit: mm)

Fig. 3: Star shaped defects in center of ingot cross section

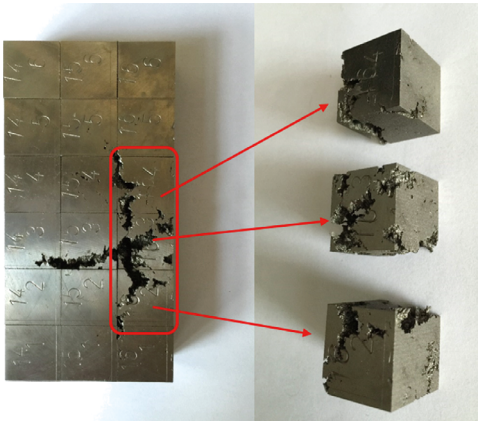

Fig. 4: Sampling of cubic billets from stock near defects area

2.3 X-ray high energy industrial CT

X-ray high energy industrial CT was used to carry out the transparent tomography image of the star shaped defects. Thousands of cross section images were stitched together by software and the porosities in the billets were counted quantitatively.

Figure 5(a) shows the six cubic samples containing the star shaped defects, and Fig. 5(b) shows the 3D CT reconstruction of the six samples, in which the porosity of each billet was counted respectively. The color intensity represents the volume rate of the continuum. The results show that the porosity rate of the six cubic samples is 8.53%, 13.24%, 11.00%, 20.28%, 34.40% and 11.77%, respectively, and the average porosity is about 16%. Figure 5(c) shows recombination of the six CT reconstructions, which perfectly reproduces the 3D solid structure with porosities of the test specimen. Figure 5(d) is the transparent view of the recombination, i.e., the negative image of solid in Fig. 5(c), which provides a totally new perspective to observe the internal structure of the porosity defects. From Fig. 5(d), both the interconnection structure and defects volume can be characterized quantitatively.

2.4 SEM

Morphology near the defects tip was inspected by using a JSM-6301F scanning electron microscope and is shown in Fig. 6, where typical hot cracking characteristics are presented.

Figure 6(a) shows an overall view of a hot crack with a meandering propagation path whose thickness decreases along the growth direction. Figure 6(b) shows a fully opened hot crack. According to the liquid film theory of hot crack [21], this is the state left by the opening of liquid film, which cannot be

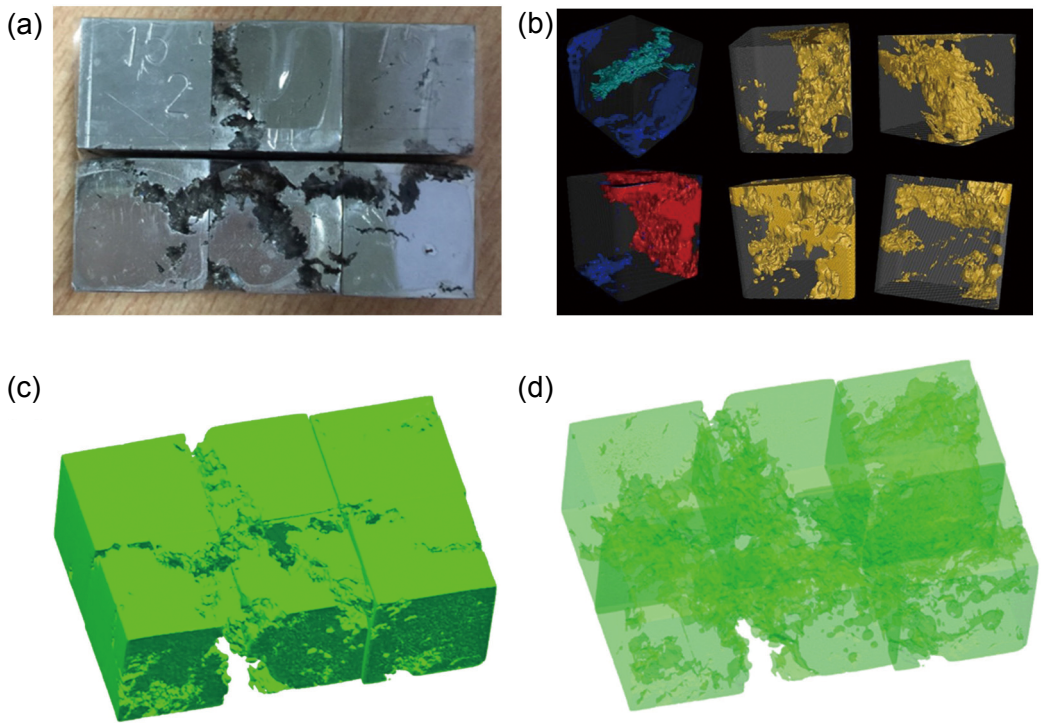

Fig. 5: Meshed samples for CT testing (a); 3D CT reconstruction of meshed samples (b); recombination of meshed CT samples (c); transparent view of recombination samples (d)

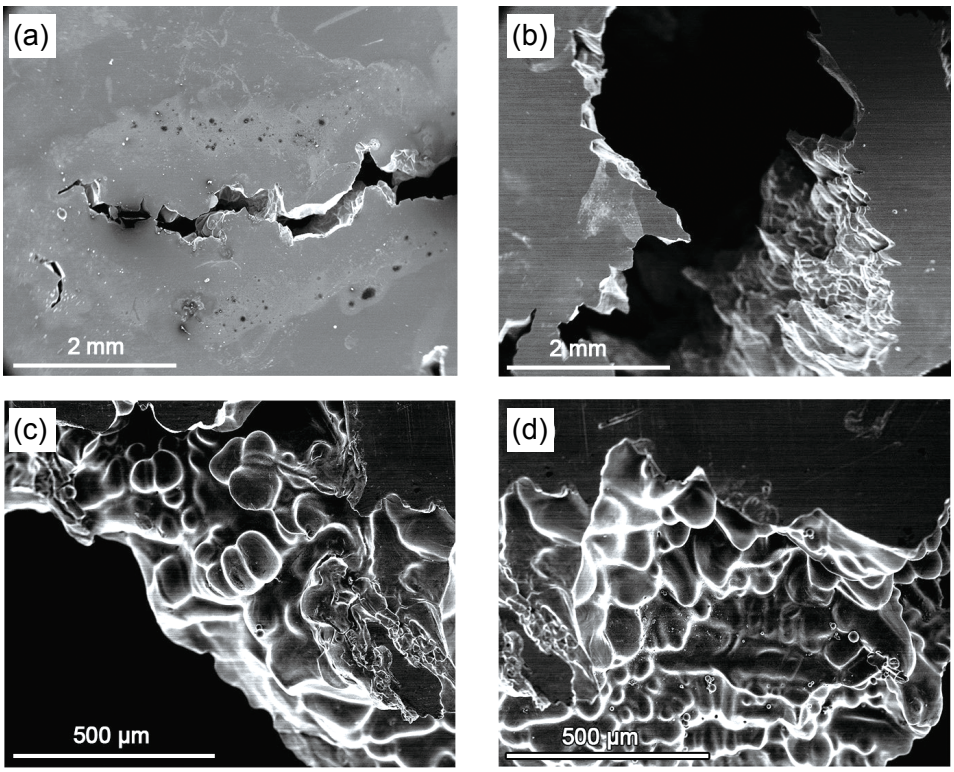

Fig. 6: Overall view of a hot crack (a), a fully opened hot crack (b), and exposed dendrite arms around hot crack (c) and (d)

fed by the liquid at the end of solidification. In Figs. 6(c) and (d), obvious exposed dendrite arms can be observed. These dendrite arms in both sides of the liquid film are torn apart by the tensile stress before they can coalesce with each other.

According to the above experimental results, the defect found in such a water-cooled ingot is called an internal shrinkage crack, because the inside root of the defect is more like shrinkage porosity while the outside tip of the defect is more like crack.

2.5 High temperature confocal microscope

To account for the influence of grain size on hot cracking potential, it is necessary to investigate the grain states at different cooling rates, which have not been torn apart by tensile stress. Therefore, the high temperature confocal microscope of Lasertec Company was used to study the macrostructure evolution during the solidification process of P91 steel, and the results were then compared and calibrated with numerical ones. The size of the samples was Φ7 mm×2.5 mm. To match the cooling rate in the core and side wall of ingot at the sampling height, 5 °C·min^{-1} and 500 °C·min^{-1} were adopted, respectively.

The samples in the ceramic crucible were heated above liquidus of the P91 steel, and then cooled down to complete solidification at set cooling rates. Finally, the samples were inspected with the optical microscope, and the grain sizes were counted as shown in Fig. 7. The average grain size is 2,200 μm at the core of the water-cooled ingot with the cooling rate of about 5 °C·min^{-1}, as shown in Fig. 7(a), and the average grain size is 500 μm at the side wall of the ingot with the cooling rate of about 500 °C·min^{-1}, as shown in Fig. 7(b).

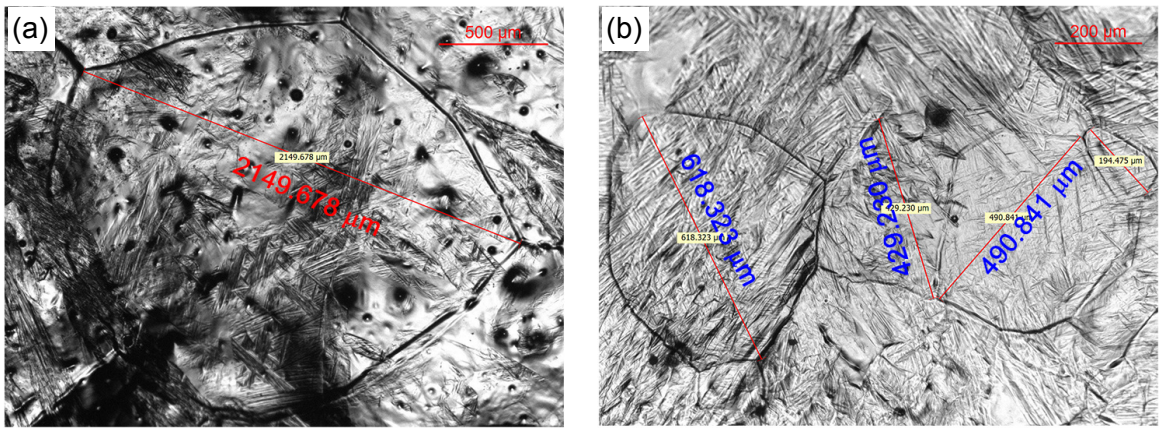

Fig. 7: Grain size results of ingot center (a) and side wall (b) tested by high temperature confocal microscope

3 Numerical simulation

In numerical simulation, the water-cooled ingot system was simplified as water-cooled inner mold, ingot, hanging insulation board, exothermic compound, anti-piping compound, and bottom casting tube. The calculation domain was meshed with 171,282 nodes and 688,061 elements, as shown in Fig. 8, in which the mesh was non-uniform, tetrahedral and 20 mm in average size.

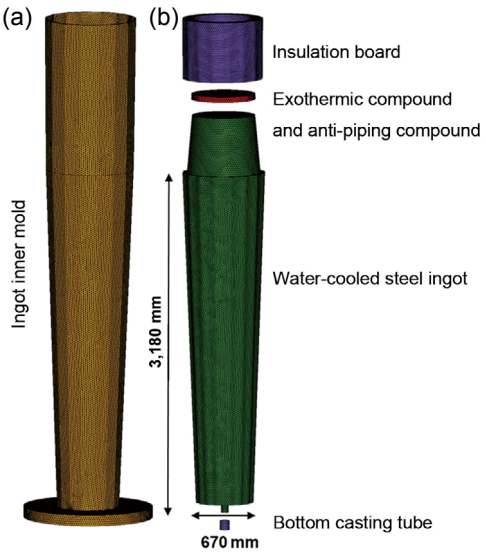

Fig. 8: 3D FEM mesh of ingot inner mold (a) and ingot system (b)

The filling process was firstly simulated, and then the thermo-mechanical simulation with macrostructure evolution was carried out to complete solidification. Viscoelastic-plastic model and air gap formation model were utilized on the ProCAST platform. The water-cooled inner mold and the hanging insulation board were assumed as rigid. The exothermic compound and anti-piping compound were combined as one entity. The initial calculation condition was confirmed according to the above production parameters, and the water-cooling boundary condition was realized by the user subroutine function.

Some of the thermophysical parameters were calculated based on the composition of P91 steel, including temperature dependent thermal conductivity, density, enthalpy, and solid fraction. Other thermophysical parameters were obtained from the high temperature mechanical experiment [22], including Young's modulus, Poisson's ratio, yield strength, secant thermal expansion coefficient, plastic modulus, viscosity coefficient, and viscosity index. The time step was adaptive, and the maximum time step was 1 s.

3.1 Shrinkage porosity

Shrinkage porosity was predicted by a dynamic refinement model [8] and Niyama criterion [14] based on ProCAST platform. The value of Niyama criterion (Ny) is shown in Eq. (1).

$$\mathrm{Ny} = \frac{G}{\sqrt{\dot{T}}} \tag{1}$$

where, G is the temperature gradient, $\dot{T}$ is the cooling rate. The smaller Niyama criterion value indicates the greater possibility of shrinkage porosity.

3.2 Hot cracking

3.2.1 Clyne and Davies criterion and Katgerman criterion

To predict the hot cracking, after completing the solidification computation of the ingot, the isochrones data from ProCAST were extracted and post-processed to obtain the Clyne and Davies (CD) criterion [23] and Katgerman (Kat) criterion [24], as shown in Eqs. (2) and (3), respectively.

$$\mathrm{HCS}_{\mathrm{CD}} = \frac{t_{\mathrm{V}}}{t_{\mathrm{R}}} = \frac{t_{0.99} - t_{0.9}}{t_{0\,9} - t_{0\,4}} \tag{2}$$

where HCS represents hot cracking susceptibility, $t_{0.99}$ is the solidification time when the volume fraction of solid, f_s, is 0.99, $t_{0.9}$ is the time when f_s is 0.9, and $t_{0.4}$ is the time when f_s is 0.4.

$$\mathrm{HCS}_{\mathrm{Kat}} = \frac{t_{\mathrm{V}}}{t_{\mathrm{R}}} = \frac{t_{0.99} - t_{\mathrm{cr}}}{t_{\mathrm{cr}} - t_{\mathrm{coh}}} \tag{3}$$

where t_{coh} is the solidification time when f_s is at the coherency point, and t_{cr} is the time when feeding becomes inadequate.

3.2.2 Hot cracking potential criterion

Hot cracking is related to solidification macrostructure and stress-strain evolution which are sensitive to the cooling intensity, especially in water-cooled conditions. Therefore, grain size distribution and mushy zone mechanical behavior within the brittle temperature range are considered.

Based on the results of high temperature confocal microscope examination, nucleation parameters were determined with the average undercooling (ΔT_μ) of 12 K, the undercooling variance (ΔT_σ) of 2.2 K, and the maximum nucleation density (n_{max}) of 1×10^9 m^{-3}. Further, considering the mushy zone mechanical behavior, a stress-based hot cracking potential (HCP) criterion is proposed to evaluate the hot cracking potential. Then, the temperature, element composition, stress, strain, and grain size distribution data were extracted from ProCAST software and post-processed to obtain the hot cracking potential criterion, which counts on the ratio of the first principal stress to the dynamic yield stress limit of mushy zone within the brittle temperature range (BTR) and the grain size distribution, as shown in Eq. (4):

$$\mathrm{HCP} = \underset{BTR}{\mathrm{Max}}\left(\frac{\sigma_{\mathrm{I}}}{\sigma_{\mathrm{dy}}}\right)\cdot g_{\mathrm{s}} \tag{4}$$

where σ_I is the first principal stress, σ_{dy} is the dynamic yield stress limit, and g_s is the grain size. The greater HCP value means the greater hot cracking potential. The dynamic yield stress limit is the modified Ludwik equation [25], as shown in Eq. (5):

$$\sigma_{\mathrm{dy}} = \sigma_0\left(1+\frac{\varepsilon_{\mathrm{eq}}}{\varepsilon_0}\right)^n\left(1+\frac{\dot{\varepsilon}_{\mathrm{eq}}}{\dot{\varepsilon}_0}\right)^m \tag{5}$$

where σ_0 is the initial yield stress, which is a function of

temperature, i.e., $0.5729-1.461\times10^{-5}T$ (MPa); T is temperature, n is the strain hardening exponent, i.e., $0.2457-6.192\times10^{-5}T$; m is the strain rate sensitivity exponent, i.e., $0.0492+9.930\times10^{-5}T$, ε_{eq} is the equivalent plastic strain, $\dot{\varepsilon}_{eq}$ is the equivalent plastic strain rate, ε_0 is the reference shear strain and $\dot{\varepsilon}_0$ is the reference shear strain rate. ε_0, $\dot{\varepsilon}_0$ and $\dot{\varepsilon}_{eq}$ are shown in Eqs. (6), (7) and (8), respectively:

$$\varepsilon_0 = \frac{\sigma_0 n}{E} \tag{6}$$

$$\dot{\varepsilon}_0 = A\,\mathrm{e}^{-Q/\mathrm{R}T} \tag{7}$$

$$\dot{\varepsilon}_{eq} = \frac{\varepsilon_{eq}}{BTR}\dot{T} \tag{8}$$

where E is the Young's modulus; A is a prefactor with value of $24{,}870+124{,}600(\%C)+12{,}400(\%C)^2\cdot s^{-1}$, in which %C is the percentage of carbon element; Q is the activation energy with value of 353 $kJ\cdot mol^{-1}$; R is the universal gas constant; $\dot{T}$ is the cooling rate. According to Eqs. (5) through (8), the larger BTR indicates the more vulnerable mushy zone.

4 Results and discussion

Figure 9(a) shows the shrinkage porosity in a water-cooled ingot based on solidification simulation, where a slender defects zone is predicted. Figure 9(b) shows the corresponding value of Niyama criterion. It can be seen that the center area in ingot with Niyama criterion below 30 $K^{0.5}\cdot s^{0.5}\cdot cm^{-1}$ [Fig. 9(b)] is consistent with that with shrinkage porosity below 0.5% [Fig. 9(a)]. Compared with the ultrasonic inspection results in Fig. 2, the simulated defects in bottom positions are more accurate, while the top positions in Figs. 9(a) and (b) are overestimated. Besides, both simulated defects' widths are underestimated, because the defects zone

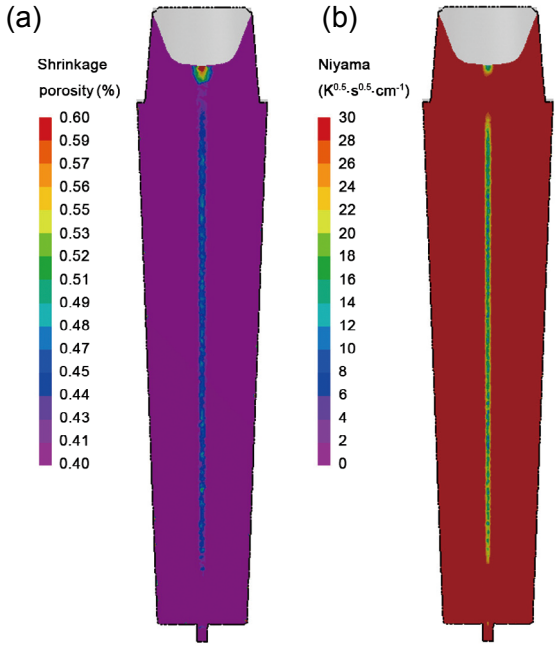

Fig. 9: Simulation results of shrinkage porosity (a) and Niyama criterion (b)

contains both shrinkage porosity and hot crack. The shrinkage porosity criterion has limitation in prediction of such defects due to its derivation. Hot crack originates from porosities formed by insufficient mass feeding, and propagates under excessive tensile stress. Therefore, the hot cracking zone is usually larger than the shrinkage porosity zone. According to the experiment, ultrasonic signals 150 mm below the ingot surface may indicate the end of hot crack connected to the porosity.

The results of CD criterion and Katgerman criterion are shown in Figs. 10(a) and (b), respectively. Since the two criteria both judge the hot cracking susceptibility by the ratio of the vulnerable time t_V (when hot cracks may develop) to the time available for the stress relief process t_R (when mass and liquid feeding occur), two simulated results are very similar with different critical times. The CD criterion and Katgerman criterion successfully predict the hot cracking in the ingot center line, but overestimate the hot cracking susceptibility in the ingot chilled layer. In fact, there are no visible hot cracks on the side wall and bottom of the ingot. The possible reason is that the cooling rate in the ingot chilled layer is too rapid and it is inadequate for the cracking prediction. These two criteria are based on non-mechanical characteristics, and have limitations.

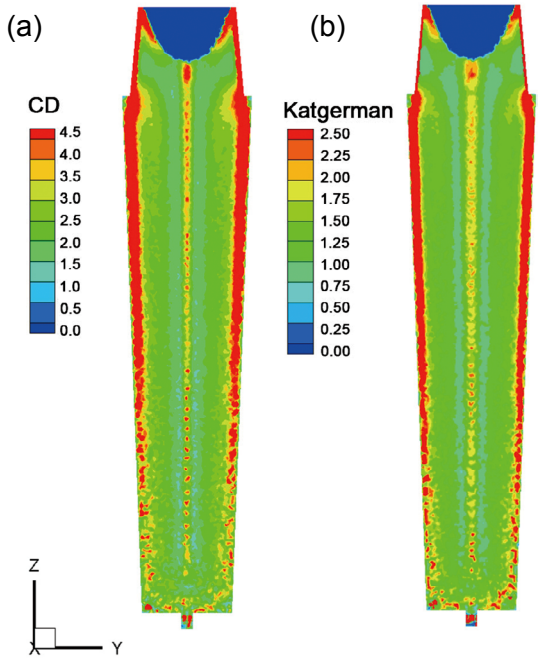

Fig. 10: Simulated hot cracking susceptibility with Clyne and Davies criterion (a), and Katgerman criterion (b)

Figure 11(a) shows the simulated grain size distribution with large size in the core and the upper part, and small size in the side wall and the lower part of ingot. The result of HCP criterion is shown in Fig. 11(b), in which the positive value means tensile stress and the negative value means compressive stress. Compared with the CD and Katgerman criteria (Fig. 10), the HCP criterion also successfully predicts the hot cracking in the ingot center, and avoids overestimation of the hot cracking in the ingot chilled layer. As shown in Fig. 2, the ultrasonic inspection results reveal that the ultrasonic signal is shallow

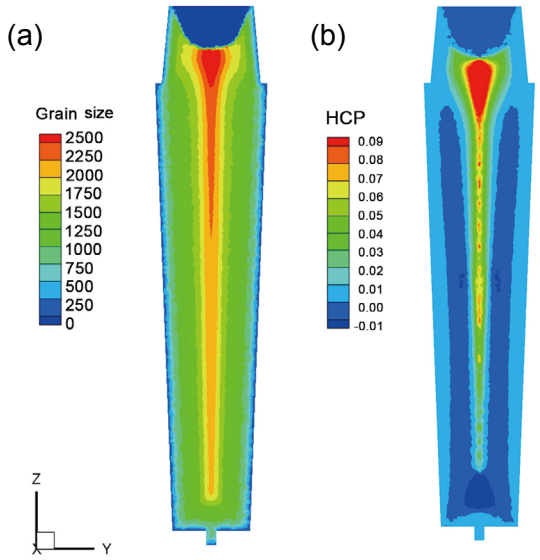

Fig. 11: Simulated grain size distribution (a), and hot cracking potential (b) in ingot

in the ingot upper part and deep in the ingot lower part. The simulation results of HCP criterion reflect the inverted cone shape of the defects zone, and more accurately predict the lower position of the defects. Since the numerical model does not cover the healing effect of molten steel feeding in the riser, the hot cracking potential is overestimated in the ingot upper part.

Through the above observation and simulation, a scenario can be inferred for the internal shrinkage crack during solidification of the water-cooled steel ingot with a large height-to-diameter ratio. Firstly, a deep shrinkage porosity band generates along the ingot center line due to lack of mass feeding, then liquid films around the porosities are torn apart due to excessive tensile stress within the BTR, and finally, hot cracks propagate along grain boundaries where the stress is concentrated. The large grain size locates in the upper and center of ingot, and allows for easy crack propagation. Therefore, the defects zone presented a deep inverted cone shape in such a water-cooled ingot with a large height-to-diameter ratio. In order to accurately predict the defects distribution of the steel ingot, it is necessary to further consider the formation and development of the defects, the healing effect of molten steel feeding and other relevant physical processes.

5 Conclusion

A 10 t water-cooled steel ingot with a large height-to-diameter ratio was cast and sectioned. By ultrasonic inspection, a deep inverted cone shape defect area was found 480 mm below the riser and 180 mm above the bottom and 150 mm in average depth beneath the surface of ingot. High energy CT and SEM indicated that the star shaped defect is internal shrinkage crack, and its root is more like shrinkage porosity while its tip is more like crack. The shrinkage crack is internally connected. Porosity generates along the ingot center line, and cavities are torn apart to crack. The grain size in the upper and center of ingot is large, and it is 500 μm in the side wall and 2,200 μm in the center of ingot, respectively.

Thermo-mechanical simulation shows that a deep shrinkage porosity forms in the centerline of the slender ingot and its height and bottom position are generally in agreement with the ultrasonic inspection results. Critical solidification time-based criterion overestimates the hot cracking potential in the ingot chilled layer, and cannot reflect the inverted cone characteristics of the defects. With consideration of macrostructure and mechanical behavior in brittle temperature of solidification, the hot cracking potential criterion can successfully reflect the inverted cone characteristics of the defects and avoid overestimation of hot cracking in the ingot chilled layer. Due to lack of consideration of the healing effect in the riser, the hot cracking potential criterion causes an overestimation of hot cracking potential in the ingot upper part.

Acknowledgements

This work was financially supported by the NSFC-Liaoning Joint Fund (Grant No. U1508215) and the project "To Strengthen Industrial Development at the Grass-Roots Level of MIIT China" (Grant No. TC160A310/21). Additionally, assistance from the Special Material Institute of Inner Mongolia North Heavy Industries Group Co., Ltd. is acknowledged.

References

[1] Liu D R, Kang X H, Sang B G, et al. Numerical study of macrosegregation formation of ingot cast in normal sand mold and water-cooled sand molds. Acta Metallurgica Sinica (English Letters), 2011, 24(1): 54–64.
[2] Meng Q Y, Wang F M, Li C R, et al. Numerical simulation of macrosegregation in water-cooled heavy flat ingot during solidification. JOM, 2014, 66(7): 1166–1174.
[3] Zhao Z G, Qiu S T, Zhu R. Comparison between the microstructures of M2 steel cast by the water-cooled copper mould and the sand mould. Chinese Journal of Engineering, 2016, 38(6): 787–794. (In Chinese)
[4] Wen C Y, Ao G W, Zhang Z S. Simulation study on the influence of bottom sub-regional cooling on 45 tons unidirectional solidification of steel ingot. Metalurgija, 2020, 59(4): 463–466.
[5] Tyurin V A, Lukanin Y V, Morozov A V. Ingot molds for obtaining long cylindrical ingots and features of the macrostructure of the metal. Metallurgist, 2013, 56(9–10): 742–747.
[6] Chen L F, Luan Y K, Li D Z, et al. Solid feeding mechanism and its application on castings with large height-to-diameter ratio. Acta Metallurgica Sinica, 2016, 52(12): 1510–1516. (In Chinese)
[7] Yu Z Y, Zhang H, Wang X B, et al. Study on heat transfer characteristics during solidification of 18-ton steel ingot with large ratio of height to diameter. Metallurgia Italiana, 2020(5): 37–47.
[8] Pequet C, Gremaud M, Rappaz M. Modeling of microporosity, macroporosity, and pipe-shrinkage formation during the solidification of alloys using a mushy-zone refinement method: Applications to aluminum alloys. Metallurgical and Materials Transactions A, 2002, 33(7): 2095–2106.
[9] Kou S. A criterion for cracking during solidification. Acta Materialia, 2015, 88: 366–374.

[10] Suyitno S T, Kool W H, Katgerman L. Integrated approach for prediction of hot tearing. Metallurgical and Materials Transactions A, 2009, 40(10): 2388–2400.
[11] Hiebler H, Bernhard C. Mechanical properties and crack susceptibility of steel during solidification. Steel Research, 1999, 70(8): 349–355.
[12] Monroe C, Beckermann C. Prediction of hot tearing using a dimensionless Niyama criterion. JOM, 2014, 66(8): 1439–1445.
[13] Koshikawa T, Bellet M, Gandin C A, et al. Study of hot tearing during steel solidification through ingot punching test and its numerical simulation. Metallurgical and Materials Transactions A, 2016, 47(8): 4053–4067.
[14] Niyama E, Uchida T, Morikawa M, et al. Method of shrinkage prediction and its application to steel casting practice. AFS International Cast Metals Journal, 1982, 7(3): 52–63.
[15] Hardin R A, Beckermann C. Effect of porosity on the stiffness of cast steel. Metallurgical and Materials Transactions A, 2007, 38(12): 2992–3006.
[16] Hardin R A, Beckermann C. Effect of porosity on deformation, damage, and fracture of cast steel. Metallurgical and Materials Transactions A, 2013, 44(12): 5316–5332.
[17] Won Y M, Yeo T J, Seol D J, et al. A new criterion for internal crack formation in continuously cast steels. Metallurgical and Materials Transactions B, 2000, 31(4): 779–794.
[18] Stangeland A, Mo A, M'Hamdi M, et al. Thermal strain in the mushy zone related to hot tearing. Metallurgical and Materials Transactions A, 2006, 37(3): 705–714.
[19] Yang J A, Shen H F, Liu B C, et al. Analysis of internal crack in a six-ton P91 ingot. China Foundry, 2016, 13(3): 191–198.
[20] Yang J A, Wang Y Q, Shen H F, et al. Numerical simulation of central shrinkage crack formation in a 234-t steel ingot. China Foundry, 2017, 14(5): 365–372.
[21] Rappaz M, Jacot A, Boettinger W J. Last-stage solidification of alloys: Theoretical model of dendrite arm and grain coalescence. Metallurgical and Materials Transactions A, 2003, 34(3): 467–479.
[22] Yang J A, Liu B C, Shen H F. Study of hot cracking potential in a 6-ton steel ingot casting. Metallurgical Research and Technology, 2018, 115(3): 308.
[23] Suyitno S T, Kool W H, Katgerman L. Hot tearing criteria evaluation for direct-chill casting of an Al-4.5 pct Cu alloy. Metallurgical and Materials Transactions A, 2005, 36(6): 1537–1546.
[24] Katgerman L. Mathematical model for hot cracking of aluminum alloys during D.C. casting. JOM, 1982, 34(2): 46–49.
[25] Galles D, Monroe C A, Beckermann C. Measurement and simulation of deformation and stresses in steel casting. IOP Conference Series: Materials Science and Engineering, MCWASP XIII: International Conference on Modeling of Casting, Welding and Advanced Solidification Processes, Schladming, Austria, 2012, 33: 012049.